Pressure-induced magnetic moment collapse and insulator-to-semimetal transition in $BiCoO_3$

2009 J. Phys.: Condens. Matter 21 295902

(http://iopscience.iop.org/0953-8984/21/29/295902)

J. Phys.: Condens. Matter **21** (2009) 295902 (8pp) doi:10.1088/0953-8984/21/29/295902

Pressure-induced magnetic moment collapse and insulator-to-semimetal transition in $BiCoO_3$

Xing Ming[1], Xing Meng[1,2], Fang Hu[1], Chun-Zhong Wang[1], Zu-Fei Huang[1,3], Hou-Gang Fan[1,4] and Gang Chen[2,3,5]

[1] Department of Materials Science, College of Materials Science and Engineering, Jilin University, Changchun 130012, People's Republic of China
[2] State Key Laboratory of Superhard Materials, Jilin University, Changchun 130012, People's Republic of China
[3] College of Physics, Jilin University, Changchun 130012, People's Republic of China
[4] College of Physics, Jilin Normal University, Siping 136000, People's Republic of China

E-mail: gchen@jlu.edu.cn

Received 18 December 2008, in final form 17 May 2009
Published 3 July 2009
Online at stacks.iop.org/JPhysCM/21/295902

Abstract

The structural stability, magnetic properties and electronic structure of tetragonal $BiCoO_3$ under pressure have been studied by first-principles density functional calculations. The calculated results reveal that no tetragonal-to-cubic and ferroelectric-to-paraelectric phase transitions occur up to 30 GPa with a volume compression of about 25%. An electronic spin crossover transition of the Co^{3+} ion from the high-spin to nonmagnetic low-spin configuration (magnetic moment collapse) occurs at 4 GPa by about 4.87% volume compression, which is concomitant with a first-order isosymmetric transition and an insulator-to-semimetal transition. The metallization in $BiCoO_3$ is driven by the spin-state transition at high pressure. Coexistence of the structural, spin-state and insulator-to-semimetal transitions implies that there is a strong coupling among the lattice, spin and charge degrees of freedom in $BiCoO_3$.

(Some figures in this article are in colour only in the electronic version)

1. Introduction

Due to the interplay between charge, spin, orbital and lattice degrees of freedom, transition metal oxides (TMOs) exhibit profuse phenomena and exotic properties, such as colossal magnetoresistance (CMR), high-temperature superconductivity, ferroelectricity and multiferroicity [1, 2]. Ferroelectric (FE) and multiferroic materials have attracted considerable attention due to the technological importance and fascinating fundamental physics [3–6]. Multiferroic materials exhibit a spontaneous magnetic polarization that can be switched through an applied electric field, and spontaneous electric polarization that can be switched through an applied magnetic field [3]. Special device applications have been suggested widely for such multiferroic materials including multiple state memory elements, electric field controlled ferromagnetic resonance devices and variable transducers with either magnetically modulated piezoelectricity or electrically modulated piezomagnetism [7, 8].

The recent revival of interest in multiferroic materials has stimulated developments of the preparation of high-quality single-crystalline samples, advances in thin-film growth techniques, and collaborations between theory and experiments [5, 9–11]. In the process of searching for new multiferroic materials, a simple insulating perovskite oxide $BiCoO_3$ has been synthesized through high-temperature and high-pressure (HP) routes [12]. $BiCoO_3$ is isostructural with tetragonal $PbTiO_3$ (space group $P4mm$) and the Co^{3+} ($3d^6$) ion adopts high-spin configurations at ambient conditions. Isolated layers of corner-shared CoO_5 pyramids are formed due to strong tetragonal distortion and the loss of the inverse center. The tetragonality ($c/a = 1.27$, where a and c are the lattice constants) of $BiCoO_3$

[5] Author to whom any correspondence should be addressed.

is much larger than that of $PbTiO_3$, which indicates a larger FE polarization (P_s) [12]. First-principles Berry-phase calculations evaluated a giant electric polarization of 179 μC cm^{-2} for $BiCoO_3$ [13, 14]. *Ab initio* density functional theory (DFT) calculations on the electronic structure and magnetic properties of tetragonal phase $BiCoO_3$ revealed that the insulating C-type antiferromagnetic (C-AFM) structure was the most stabilized among all possible spin configurations from the viewpoint of energy [12–15]. A neutron powder diffraction (NPD) experiment unambiguously confirmed that $BiCoO_3$ is a C-AFM insulator below the Néel temperature (T_N) of 470 K [12]. Therefore, tetragonal phase $BiCoO_3$ is a promising candidate for a multiferroic material exhibiting both ferroelectricity and antiferromagnetism simultaneously.

Density functional calculations are employed extensively to investigate, explore and predict the behavior of condensed-matter systems under pressure. For example, the pressure-induced structural phase transition, magnetic moment collapse and insulator–metal transition (IMT) in the typical TMO MnO have been investigated intensively by first-principles DFT calculations [16–19]. Recently, the pressure-induced anomalous phase transitions, morphotropic phase boundaries (MPBs) and giant enhancement of piezoelectricity in $PbTiO_3$ have been debated intensively by DFT calculations [20–23]. *Ab initio* simulations have revealed an unimaginable reappearance of the ferroelectricity in perovskites and related materials at ultra-high pressure [24, 25]. First-principles study was reported to explain the pressure-induced IMT, volume collapse and spin crossover in $BiFeO_3$ [26].

Ravindran *et al* reported that magnetic instability can induce strong magneto-electric coupling in $BiCoO_3$ based on *ab initio* electronic structure calculations [14]. In this work, *ab initio* DFT calculations are also performed to investigate pressure-induced structural, electronic and magnetic effects in tetragonal $BiCoO_3$. At ambient conditions, the ground state of the tetragonal $BiCoO_3$ is confirmed to be the C-AFM state by total energy calculations. At 4 GPa, a spin crossover transition from the high-spin (HS) to nonmagnetic low-spin (LS) state occurs accompanied by an isosymmetric first-order structural phase transition, which is concurrent with an insulator-to-semimetal transition. The low-spin phase of the tetragonal $BiCoO_3$ is stable up to 30 GPa and tetragonal-to-cubic phase transformation has not occurred.

2. Computational methods

The *ab initio* calculations are carried out by employing the DFT plane-wave (PW) pseudopotential method encoded in the CASTEP code [27] using the spin-polarized generalized gradient approximation (GGA) [28] and Vanderbilt-type ultrasoft pseudopotential (USP) [29]. The initial crystal structure model of tetragonal $BiCoO_3$ is built according to the NPD data [12]. After careful convergence testing, the PW cut-off energy is set to 750 eV; requested k-point spacing is fixed to 0.03 Å^{-1} for all calculations. Geometry optimizations are performed to fully relax the atomic internal coordinates and the lattice parameters within the BFGS minimization algorithm [30]. The convergence thresholds for energy change, maximum force, maximum stress, and maximum displacement between optimization cycles are 5×10^{-6} eV/atom, 0.01 eV Å^{-1}, 0.02 GPa and 5×10^{-4} Å, respectively.

Table 1. Calculated energies of various spin ordering states for tetragonal FE $BiCoO_3$ (the C-AFM state is set as the reference with the lowest energy), which are compared with other theoretical results (energies are given in eV/formula unit (f.u.)). The columns 'Expt' and 'Relx.' are calculated results for the NPD experiment determined crystal structure [12] and geometry relaxed structure, respectively.

	FP-LAPW LSDA[a]	FP-LAPW GGA[b]	FP-LAPW LSDA[b]	PAW[c]	USP-PW GGA[d]	
					Expt	Relx.
FM	0.37	0.340	0.345	0.268	0.291	0.292
A-AFM	0.46	0.215	0.205	0.120	0.229	0.249
C-AFM	0	0	0	0	0	0
G-AFM	0.03	0.073	0.039	0.028	0.031	0.023

[a] Taken from [13].
[b] Taken from [15].
[c] Taken from [14].
[d] Present calculation.

3. Results and discussion

3.1. Ground state at ambient conditions

The ground state of the tetragonal FE phase $BiCoO_3$ is determined by considering four possible spin configurations, ferromagnetic (FM) and A- (C-, G-) type AFM (A-AFM, C-AFM and G-AFM) ordering. All magnetic moments are aligned parallel in the FM state for a crystallographic primitive cell, FM ab planes stacked antiferromagnetically along the c direction in the A-AFM state for a $1 \times 2 \times 1$ supercell, AFM ab planes stacked ferromagnetically along the c direction in the C-AFM state for a $\sqrt{2} \times \sqrt{2} \times 1$ supercell, and AFM along all three directions in the G-AFM state for a $\sqrt{2} \times \sqrt{2} \times 2$ supercell. Structural relaxations are performed for all four spin ordering states before the electronic structure calculations. The calculated total energies of the four spin configurations are listed in table 1. The total energy of the C-AFM state is the lowest among all magnetic ordering phases, which is consistent with other theoretical calculated results [13–15]. Our DFT calculations confirm the C-AFM magnetic ordering state to be the ground state of the tetragonal FE phase $BiCoO_3$ at ambient conditions, which is consistent with the NPD experiment [12].

The crystal structure model of tetragonal $BiCoO_3$ is shown in figure 1: the crystallographic primitive cell consists of a five-atom $BiCoO_3$ formula unit, and the C-AFM magnetic ground state is a ten-atom $\sqrt{2} \times \sqrt{2} \times 1$ supercell containing two $BiCoO_3$ formulae. The calculated lattice constants, atomic positions and magnetic moment for the ground state of tetragonal FE $BiCoO_3$ are listed in table 2. Our calculated results are in good agreement with available experimental data [12] and other theoretically calculated results [14, 15]. Despite a large reduction of spin moment of the Co ion in comparison with the expected value of the $3d^6$ electronic configuration (4 μ_B), the experimentally

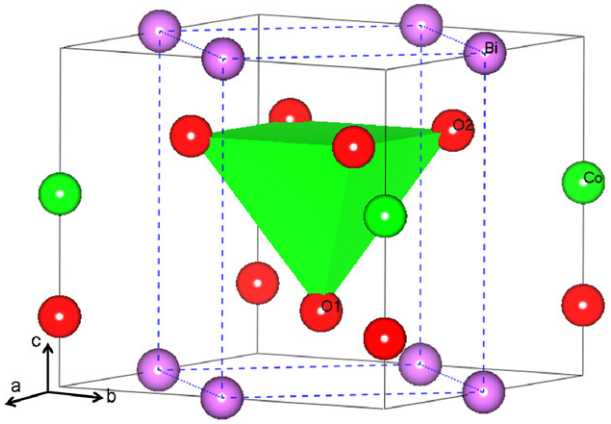

Figure 1. Crystal structural perspective polyhedral views of the ten-atom $\sqrt{2} \times \sqrt{2} \times 1$ supercell for the tetragonal phase $BiCoO_3$. The crystallographic primitive cell is marked by the dashed-line polyhedron, and the square pyramid is the schematic CoO_5 polyhedron.

Table 2. Experimentally measured and theoretically calculated lattice constants, atomic positions and magnetic moment (M) of tetragonal phase $BiCoO_3$ at ambient conditions. The atomic positions of ideal cubic phase (space group $Pm\bar{3}m$) are Bi (0, 0, 0), Co (0.5, 0.5, 0.5), O1 (0.5, 0.5, 0), O2 (0.5, 0, 0.5), and the corresponding tetragonal phase are Bi (0, 0, 0), Co (0.5, 0.5, $0.5 + \Delta z$), O1 (0.5, 0.5, Δz_1), O2 (0.5, 0, $0.5 + \Delta z_2$), respectively. For the convenience of comparison, the lattice parameters and position coordinates of the C-AFM magnetic unit cell have been transformed to those of the crystallographic primitive cell.

	Expt (5 K)[a]	Calc.[b]	Calc.[c]	Calc.[d]
a (Å)	3.7199	3.748	3.7304	3.7221
c (Å)	4.7196	4.710	4.7897	4.8551
c/a	1.27	1.26	1.28	1.30
M (μ_B)	3.24	3.0	3.10	3.08
Δz	0.0664	0.0658	0.0718	0.0745
Δz_1	0.2024	0.2053	0.2015	0.2019
Δz_2	0.2311	0.2287	0.2194	0.2265

[a] Taken from [12].
[b] Taken from [15].
[c] Taken from [14].
[d] Present calculation.

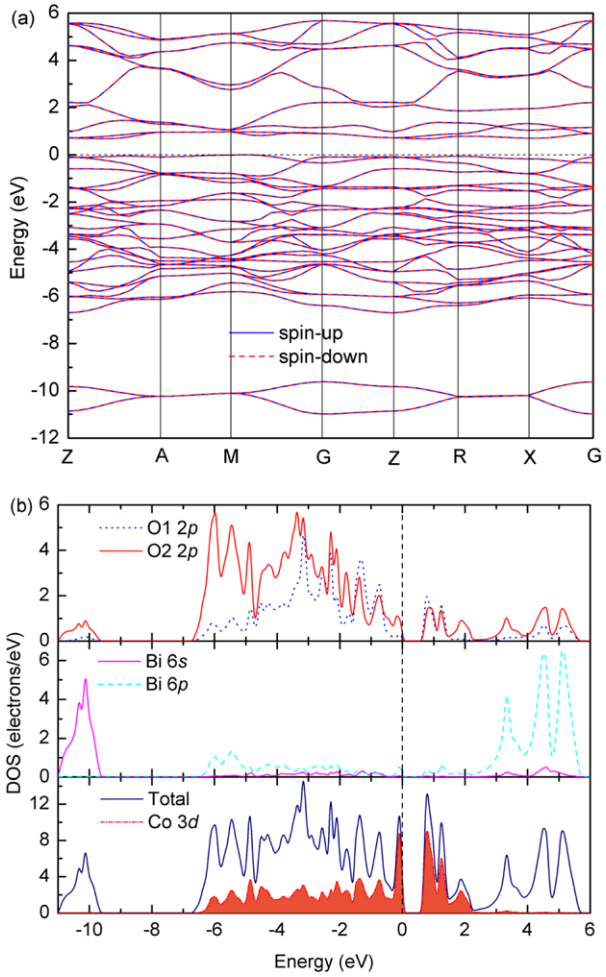

Figure 2. Ground state electronic structures of tetragonal phase $BiCoO_3$ with C-AFM spin configuration. (a) Spin-polarized band structure; the horizontal dashed line at 0 eV corresponds to the Fermi level (E_F). The spin-up/down subbands are plotted with solid/dashed lines, which overlap each other due to the AFM ordering. (b) Total and atomic-resolved projected partial density of states (PDOS); the vertical dashed line at 0 eV corresponds to E_F.

determined HS configuration of the Co^{3+} ($3d^6$) ion [12] has been successfully reproduced. The calculated spin moment residing at the Co site is 2.58 μ_B, whereas the residual magnetic moment of the O1 ion is 0.50 μ_B. The calculated total spin moment of 3.08 μ_B/f.u. is comparable with the NPD experiment measured value [12] and other theoretical calculated results [14, 15].

The band structure and corresponding total density of states (DOS) and atomic-resolved projected DOS of the tetragonal $BiCoO_3$ with C-AFM spin configuration are shown in figure 2. The elementary characteristics of the band structure are the same as those calculated by the local spin density approximation (LSDA) [15]. The most remarkable characteristic of the energy bands is that the spin-up and spin-down subbands overlap each other. These two spin states are absolutely identical at the same energy, exhibiting the unique characteristic of the AFM ordering. The lowest two pairs of degenerate valence bands are derived from the Bi 6s states approximately 10.5 eV below the Fermi level (E_F), which are split off from a manifold of occupied O 2p and Co 3d derived bands extending from −7 eV to E_F. The conduction bands above E_F are predominantly derived from Co 3d unoccupied states, which are followed by Bi 6p derived states at the higher energy region around 4 eV. The insulating band gap is about 0.67 eV between the top of the valence band and the bottom of the conduction band, which is consistent with the experimental observed insulating behavior [12]. The atomic-resolved partial DOS indicates strong hybridization effects for O 2p–Co 3d and Bi (6s, 6p)–O 2p states. The hybridizations of the Co–O1 bond induce the strong covalent effect and a large decrease of the Co ion spin moment. In addition, the hybridization effects of Co–O and Bi–O play an important role in the ferroelectric structural distortion in tetragonal FE $BiCoO_3$ [15].

The detailed features of the electronic states can be inspected clearly from the orbital-resolved DOS [15] or spin-

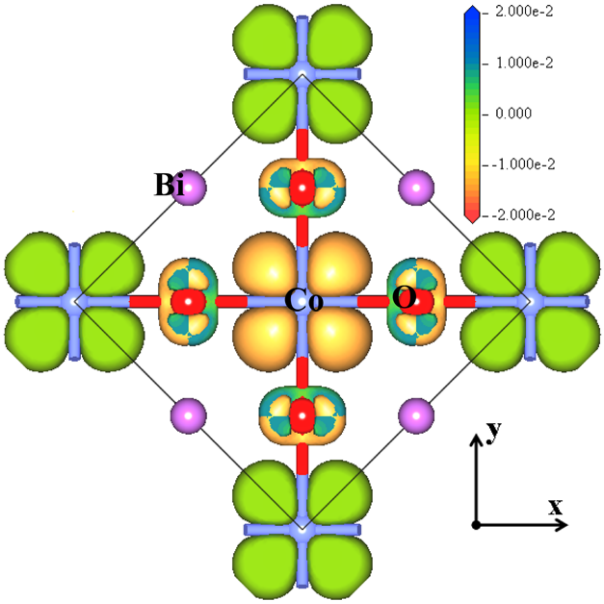

Figure 3. Orbital distributions at the top of the valence bands viewed perpendicular to the *ab* plane in tetragonal $BiCoO_3$ with C-AFM spin configuration. The positive/negative values of the legend indicate the spin-up/down states, respectively.

resolved electronic density distribution (orbitals). The 3d levels split into nondegenerate b_{2g} (d_{xy}), doubly degenerate e_g (d_{yz}, d_{zx}), nondegenerate a_{1g} (d_{z^2}), and b_{1g} ($d_{x^2-y^2}$) levels in the square-pyramidal crystal field [14]. The energy of the d_{xy} orbital is the lowest, which is separated from the other 3d orbitals by the crystal-field splitting. In addition, the intra-atomic exchange splitting (on-site Hund's coupling) promotes the spin-down states shift to higher energy relative to the spin-up ones. In the fully ionized picture, the electronic configuration of the Co^{3+} ion is $3d^6$. Therefore, the spin-up Co 3d orbitals are all occupied with HS spin configuration [12]; in contrast, only the d_{xy} orbital is exclusively occupied in the spin-down subbands, so the top of the valence bands mainly consists of Co 3d states with d_{xy} character as shown in figure 3, which is formed due to a combination of strong crystal-field splitting associated with the exchange splitting [13–15]. The insulated band gap opens up between the occupied Co d_{xy} orbital and other unoccupied d orbitals in the same spin channel. The Co d_{xy} orbitals are hybridized strongly with the O p_x/p_y orbitals in the *ab* plane forming the C-AFM magnetic coupling, and also reduce the Co ion spin moment.

3.2. Structural, electronic and magnetic transitions under pressure

Our DFT calculations confirm the ground state of the tetragonal FE phase $BiCoO_3$ to be the C-AFM state at ambient conditions. The equilibrium crystal structure of the ideal cubic paraelectric (PE) phase and the ten-atom supercell of the tetragonal FE phase are further relaxed by elaborate geometry optimization under pressure. Two possible electronic configurations of the Co^{3+} ion with $3d^6$ electronic configuration, i.e. LS ($b_{2g}^2 e_g^4 a_{1g}^0 b_{1g}^0$, $S = 0$) and HS

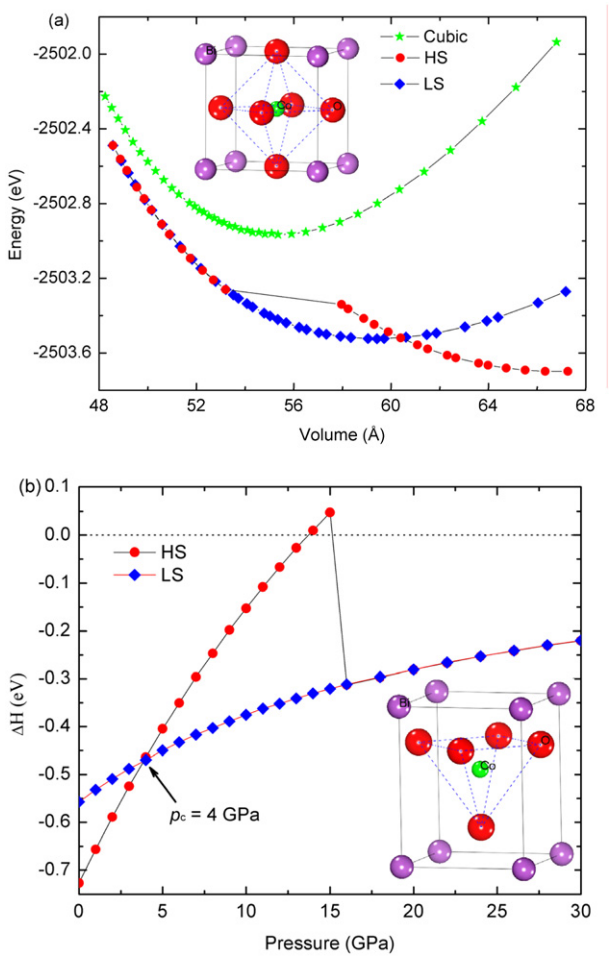

Figure 4. (a) The total energy $E(V)$ curve of the cubic PE and tetragonal FE phases at the corresponding volumes. (b) The dependence of enthalpy differences (ΔH) of the tetragonal FE phases (horizontal dashed line at 0 eV indicates the cubic PE phase used as a reference) on pressure up to 30 GPa. Inset: the unit cell crystal structures of the cubic PE (a) and tetragonal FE (b) $BiCoO_3$.

($b_{2g}^2 e_g^2 a_{1g}^1 b_{1g}^1$, $S = 2$) states [14], have been taken into account during the calculation process for the tetragonal $BiCoO_3$. The present spin-polarized DFT calculations specify artificially the LS and HS states by fixing the unpaired numbers of electrons to zero and four at the Co^{3+} ion sites for tetragonal $BiCoO_3$. This method allows the moment to float and the ground state is obtained by minimizing the energy functional with respect to the charge and magnetization densities. Ravindran *et al* calculated the total energy as a function of magnetic moment using the so-called fixed spin moment method, where they used the magnetic moment M as an external parameter and calculated the total energy as a function of M [14].

The Co^{3+} ion in cubic PE phase shows LS nonmagnetic character by electronic structure calculations. As shown in figure 4(a), the calculated total energy of the cubic PE phase is always higher than the tetragonal FE phase, which suggests the tetragonal to cubic structural transformation will not occur. However, the total energy $E(V)$ curve of the HS FE phase shows a discontinuous characteristic implying a phase transition. The superposition of the HS state with the LS state

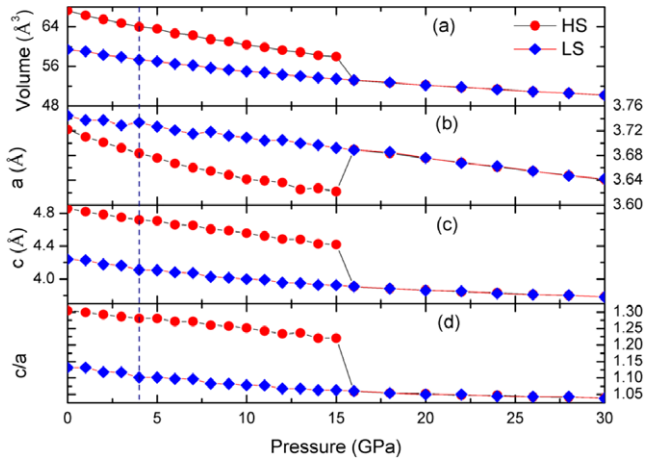

Figure 5. Pressure dependence of the (a) volume, (b) lattice constant a, (c) lattice constant c, and (d) axial ratio c/a for the HS and LS tetragonal phases of $BiCoO_3$. We give the results for all three phases in the whole pressure range, but note that the HS phase is stable only below 4 GPa and at ambient pressure, whereas the LS phase is stable above 4 GPa. Dashed vertical lines mark the calculated transition pressures.

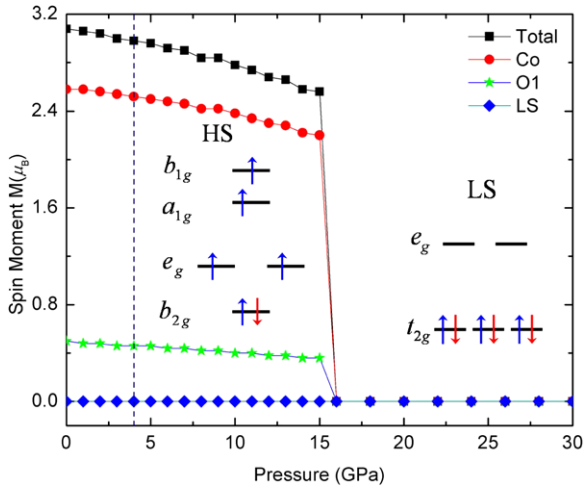

Figure 6. Variation of the spin magnetic moment (the spin moment at the O2 site is zero and not shown) with pressure for tetragonal phase $BiCoO_3$. Dashed vertical lines mark the calculated transition pressures of 4 GPa. The insets are schematic diagrams of the HS and LS spin configurations for the Co^{3+} ($3d^6$) ions in the pyramidal and distorted octahedral coordination environments, respectively.

in the $E(V)$ curve indicates the spin crossover transition from the HS state at the equilibrium volume to the LS state under pressure. Generally, the transition pressure can be calculated from the slope of a common tangent to the $E(V)$ curves of different phases. In practice, the free parameter in experiment is the pressure p applied to the sample. The corresponding thermodynamic potential is the enthalpy $H(p) = E[V(p)] + pV(p)$. It is more convenient to calculate enthalpy differences with respect to a given phase, where the transition pressure is given by the intersection of two curves [17, 23, 24, 26]. The enthalpy differences (ΔH) as a function of pressure up to 30 GPa are shown in figure 4(b). The enthalpy of the HS state displays an anomalous behavior at 15 GPa and superposes with the LS state above 16 GPa. It is obvious that the phase transition point of the spin crossover from the HS state to the LS state is about 4 GPa for the tetragonal $BiCoO_3$. In addition, the enthalpy of the cubic PE phase is always higher than that of the tetragonal LS state. The LS tetragonal phase is stable up to at least 30 GPa and the structural transformation from tetragonal to cubic phase is not observed.

Figure 5 shows the evolution of the structural parameters with pressure for the tetragonal $BiCoO_3$. All structural parameters of the HS state show a dramatic transformation at 15 GPa. The unit cell volume decreases abruptly with a volume collapse of about 7% ($\Delta V/V_0 \sim 7\%$, where V_0 is the equilibrium volume of tetragonal $BiCoO_3$ at ambient condition) at 15 GPa. The discontinuous volume contraction is accompanied by an abrupt expansion of the a axis and a sudden shrinkage of the c axis. The axial ratio c/a changes from about 1.22 to 1.05. The structure of the HS state has relaxed to the LS state above 15 GPa, which is proved by the superposition of the structural parameters. As shown in figure 4(b), the transition pressure from HS to LS state has been determined by the enthalpy difference of the tetragonal $BiCoO_3$ to be 4 GPa, and the corresponding volume compression is about 4.87%. The remarkably concurrent transformations of the structural parameters clearly indicate the first-order phase transition characteristics. The variation of the magnetic moment with pressure is presented in figure 6. The magnetic moment of the tetragonal HS $BiCoO_3$ collapses at 4 GPa, which corresponds to the spin crossover of the Co^{3+} ion from HS to nonmagnetic LS configurations. Although the structural parameters of the tetragonal $BiCoO_3$ display a prominent change at 4 GPa, the symmetry of the tetragonal $BiCoO_3$ has not altered after the spin crossover. Therefore, the transition at 4 GPa is assigned to a first-order isosymmetric phase transition.

It is well known that ferroelectricity is highly sensitive to external pressure; tetragonal to cubic (T-to-C) structural transformations associated with FE to PE phase transitions often take place for tetragonal ferroelectrics under pressure. For example, a second-order T-to-C phase transition occurs from 11.2 GPa at room temperature (RT) in $PbTiO_3$ [31]; a first-order T-to-C phase transition occurs between 1.8 and 3 GPa at RT in $BaTiO_3$ [32]. Our DFT calculations indicate no T-to-C and no FE-to-PE phase transitions occurring below 30 GPa. We note that Ravindran *et al* proposed FE-to-PE phase transitions accompanied by 17% volume change, where the first-principles DFT calculations were performed using the PAW method as implemented in the VASP code [14]. However, the present DFT calculations reveal that the tetragonal LS structure is stable up to 30 GPa, corresponding to a volume compression of about 25%.

The 3d levels split into threefold degenerate t_{2g} (d_{xy}, d_{yz}, d_{zx}) and doubly degenerate e_g ($d_{z^2}, d_{x^2-y^2}$) levels in the ideal octahedral crystal field (CF), which will split further into nondegenerate b_{2g} (d_{xy}), doubly degenerate e_g (d_{yz}, d_{zx}), nondegenerate a_{1g} (d_{z^2}), and b_{1g} ($d_{x^2-y^2}$) levels in the square-pyramidal CF as shown in the inset of figure 6 [14]. As a result of the competition among CF splitting, on-site Coulomb correlation effects and intra-atomic

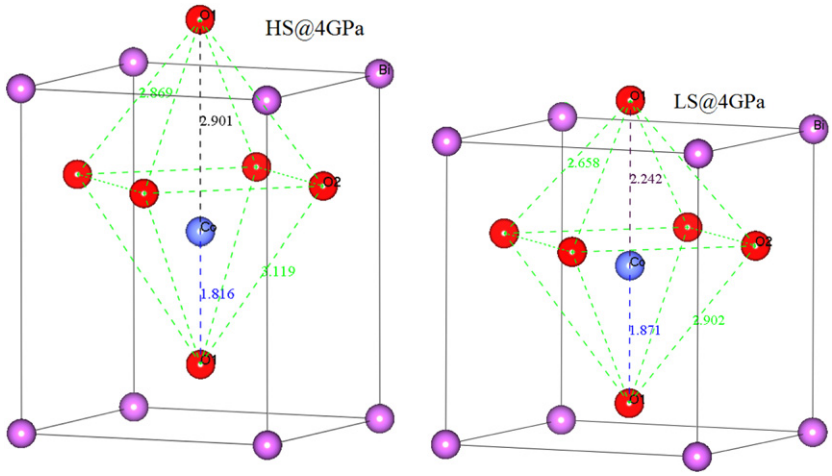

Figure 7. Transformation of the coordination environment of the Co^{3+} ions in tetragonal $BiCoO_3$ around the spin crossover. The arrises (O1–O2) of the coordination polyhedron and the Co–O bond lengths along structural distortion directions are marked, implying the coordination polyhedron changes from a CoO_5 pyramid to a distorted CoO_6 octahedron accompanied by the spin crossover from HS to LS.

Hund's rule exchange coupling, the Co^{3+} ion with CoO_5 square-pyramidal coordination can adopt three possible spin configurations, i.e. LS ($b_{2g}^2 e_g^4 a_{1g}^0 b_{1g}^0$, $S = 0$), intermediate spin (IS) ($b_{2g}^2 e_g^3 a_{1g}^1 b_{1g}^0$, $S = 1$) and HS ($b_{2g}^2 e_g^2 a_{1g}^1 b_{1g}^1$, $S = 2$) states. Likewise, three possible spin states of Co^{3+} ion, the LS ($t_{2g}^6 e_g^0$, $S = 0$), IS ($t_{2g}^5 e_g^1$, $S = 1$) and HS ($t_{2g}^4 e_g^2$, $S = 2$) states, can appear in a CoO_6 octahedral CF. Though these relevant energy scales are important for the spin states of the Co^{3+} ion, only the CF splitting is extraordinarily sensitive to pressure. It has been established that the spin-state transition is primarily controlled by competition between the CF splitting (favoring the LS state) and the intra-atomic exchange coupling (favoring the HS state) [17]. The CF splitting enhances dramatically under pressure. Therefore, the system transforms to an LS state when the CF splitting exceeds the Hund's rule exchange energy. It is generally believed that the Co^{3+} ions adopt the LS/IS state in octahedral CoO_6/pyramidal CoO_5 coordination environments [33]. However, the spin state of the Co^{3+} ion has been a controversial topic and has led to intensive debate, especially in a CoO_5 pyramidal coordination [34]. Calculated structural parameters indicate that the spin crossover transition is accompanied by a dramatic decrease of the tetragonality from 1.28 to 1.10 at 4 GPa, which drives the Co–O coordination polyhedron change from the CoO_5 pyramid to the distorted CoO_6 octahedron as shown in figure 7. The Co^{3+} ions keep on being displaced from the octahedral center of the distorted CoO_6 octahedron, and the inverse symmetry is still lost under HP. Accordingly, the increase of the CF splitting and the transformation of the coordination environment lead to the spin crossover of the Co^{3+} ions from HS to LS states. The isosymmetric volume contraction is most likely due to the moment collapse of the Co^{3+} ions, because the ionic radius of the HS state Co^{3+} ion is larger than that of the LS state [35].

The band structure and corresponding density of states (DOS) for tetragonal $BiCoO_3$ at 4 GPa are presented in figure 8, where the Fermi level (E_F) is set to 0 eV. One prominent characteristic of the band structures is that the spin-*up* and spin-*down* subbands overlap each other, which displays the AFM ordering in the HS phase and nonmagnetic characteristic in the LS phase of the tetragonal $BiCoO_3$. The essential characteristics of the band structure for the HS phase are the same as those at ambient pressure (see figure 2). The insulating band gap has reduced to 0.57 eV due to the well known bandwidth broadening under pressure. The five bands around E_F are predominated by the Co 3d states in the LS phase, which split into a lower lying t_{2g} manifold and higher lying e_g states in accordance with the CF analysis. The pseudogap feature between these Co 3d states results in a low value of DOS at the E_F as shown in figure 8(c); the E_F is located in the valley of the DOS, which reflects the stability of the LS phase of the tetragonal $BiCoO_3$. There is one valence band across the E_F forming a hole pocket around R, and one conduction band traveling across the E_F merely around the special K points of M and X forming the electron pockets. The bottom of the conduction band overlaps with the top of the valence band around E_F in a different part of momentum space (at a different K vector) forming a negative indirect band gap, which are characteristics of semimetallicity.

Pressure strongly affects the structural, transport and magnetic properties of TMO, which often leads to magnetic collapse [16–19], spin-state transition [35] and the insulator–metal transition (IMT) [26, 36]. The IMT in TMO is one of the most actively investigated themes in condensed-matter physics of correlated electron materials. Bandwidth control and band-filling control are two traditional mechanisms for the metallization of the insulator [37]. The bandwidth controlled IMT can be experimentally achieved by chemical substitution or by applying pressure, whereas the filling controlled IMT can be induced by doping of charge carriers into the parent insulator compound. The application of external pressure provides a powerful tool to tune the structural, electronic and magnetic properties of real materials [16, 17, 19, 26, 36, 38, 39]. Inspired by the pressure-driven IMT accompanied by a change of the local spin state (HS to LS crossover) in transition metal ions with $3d^5$

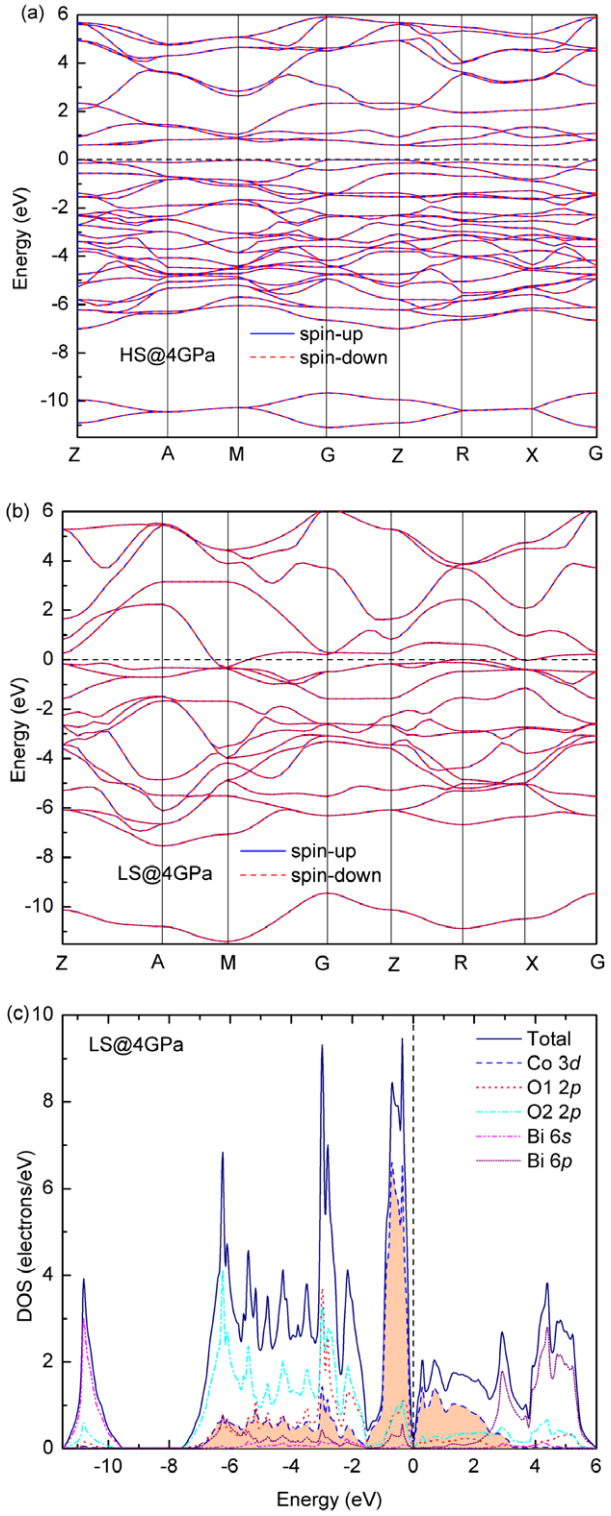

Figure 8. Variation of the electronic structure of the tetragonal $BiCoO_3$ from HS to LS state at 4 GPa: (a) the band structure for the HS phase, (b) the band structure for the LS phase and (c) the total DOS and atom-resolved partial DOS for the LS phase. O1 and O2 correspond to the apical (along the *c* axis) and equatorial (parallel to the *ab* plane) O ions in the distorted CoO_6 octahedron as shown in figure 7. The highlighted area indicates the DOS for Co^{3+} ions. Note that the HS phase is a C-AFM spin ordering magnetic cell containing two $BiCoO_3$ formulae, whereas the LS phase is nonmagnetic and corresponding to the crystallographic primitive cell (one $BiCoO_3$ formula unit).

configuration, some possible transition scenarios of IMT have been brought out recently for MnO [19], $BiFeO_3$ [36, 40] and Fe_2O_3 [39]. A different 'Hubbard energy control' mechanism of the IMT was proposed for $BiFeO_3$ [36, 40], whereas two possible scenarios of *gap closing* and *local state transition* mechanisms are suggested for Fe_2O_3 and MnO by Kuneš *et al* [39].

The present DFT electronic structure calculations reveal a spin crossover of Co^{3+} ions with simultaneous insulator-to-semimetal transition in tetragonal $BiCoO_3$ under pressure. Application of pressure induces the isosymmetric transition and the modification of the coordination environment of the Co^{3+} ions in the tetragonal $BiCoO_3$. The spin state of Co^{3+} ions changes from the HS to LS spin configuration at HP. The 3d electrons are pairwise compensated and fill in the three t_{2g} orbitals in the LS nonmagnetic state ($S = 0$). The complex phase transitions including an insulator-to-semimetal transition concurrent with the structural and spin-state transitions provide remarkable evidence of strong coupling between spin, charge and lattice degrees of freedom. We tentatively suggest that the insulator-to-semimetal transition in $BiCoO_3$ is initiated by the lattice compression and driven by the spin crossover effects at HP in contrast to the bandwidth controlled scenario. The metallization behavior in tetragonal $BiCoO_3$ is similar to the cases in MnO [19], $BiFeO_3$ [36] and Fe_2O_3 [39], where the spin degree of freedom plays an important role. However, we should note there are some notable differences between the cases in tetragonal $BiCoO_3$ and other $3d^5$ systems. In tetragonal $BiCoO_3$ there is a distinct variation of the local coordination environment of the Co^{3+} ions from the CoO_5 pyramid to the distorted CoO_6 octahedron as shown in figure 7. In contrast, the cubic crystal field for Mn^{2+} or Fe^{3+} ions in $3d^5$ systems has been unaltered. In addition, the spin crossover of Co^{3+} ions leads to the orbital and spin degrees of freedom freezing up in the nonmagnetic LS state ($S = 0$), whereas those of the LS state ($S = 1/2$) in $3d^5$ ions have not been eliminated completely. Our theoretical computational work calls for further HP experimental investigations as well as LDA + DMFT (a combination of the DFT in the local density approximation (LDA) and the dynamical mean field theory (DMFT)) calculations to further clarify the nature of the transition.

4. Conclusion

We have demonstrated that pressure induces a first-order isosymmetric transition accompanied by magnetic moment collapse in tetragonal phase $BiCoO_3$. Pressure drives the structural transformation, spin crossover of the Co^{3+} ions and insulator-to-semimetal transition simultaneously. In contrast to the two widely accepted scenarios of IMT, we propose that the metallization mechanism in $BiCoO_3$ is the spin crossover effect at HP. Due to the complicated coupling interactions of spin, charge, orbital and lattice degrees of freedom, tetragonal $BiCoO_3$ affords a ground to investigate variously intriguing characteristic and profuse phenomena. Pressure tuning of the structure, electronic structure and spin state is promising to be a fascinating avenue for experimental study.

Acknowledgments

This work was sponsored by both the Chinese National Science Foundation under grant No 50672031 and the Program for Changjiang Scholar and Innovative Research Team in University under grant No IRT0625. This work was also partially supported by the PhD program foundation of the MOE of China under grant No 20070183003 and the Scientific and Technologic Research and Development program of Jilin Province, China, under grant No 20060511.

References

[1] Tokura Y and Nagaosa N 2000 *Science* **288** 462
[2] Dagotto E 2005 *Science* **309** 257
[3] Eerenstein W, Mathur N D and Scott J F 2006 *Nature* **442** 759
[4] Spaldin N A and Fiebig M 2005 *Science* **309** 391
[5] Cheong S-W and Mostovoy M 2007 *Nat. Mater.* **6** 13
[6] Scott J F 2007 *Science* **315** 954
[7] Scott J F 2007 *Nat. Mater.* **6** 256
[8] Gajek M, Bibes M, Fusil S, Bouzehouane K, Fontcuberta J, Barthélémy A and Fert A 2007 *Nat. Mater.* **6** 296
[9] Martin L W, Crane S P, Chu Y H, Holcomb M B, Gajek M, Huijben M, Yang C H, Balke N and Ramesh R 2008 *J. Phys.: Condens. Matter* **20** 434220
[10] Hill N A 2000 *J. Phys. Chem.* B **104** 6694
[11] Spaldin N A and Pickett W E 2003 *J. Solid State Chem.* **176** 615
[12] Belik A A, Iikubo S, Kodama K, Igawa N, Shamoto S, Niitaka S, Azuma M, Shimakawa Y, Takano M, Izumi F and Takayama-Muromachi E 2006 *Chem. Mater.* **18** 798
[13] Uratani Y, Shishidou T, Ishi F and Oguchi T 2005 *Japan. J. Appl. Phys.* **44** 7130
[14] Ravindran P, Vidya R, Eriksson O and Fjellvåg H 2008 *Adv. Mater.* **20** 1353
[15] Cai M Q, Liu J C, Yang G W, Cao Y L, Tan X, Chen X Y, Wang Y G, Wang L L and Hu W Y 2007 *J. Chem. Phys.* **126** 154708
[16] Cohen R E, Mazin I I and Isaak D G 1997 *Science* **275** 654
[17] Yoo C S, Maddox B, Klepeis J H P, Iota V, Evans W, McMahan A, Hu M Y, Chow P, Somayazulu M, Häusermann D, Scalettar R T and Pickett W E 2005 *Phys. Rev. Lett.* **94** 115502
[18] Kasinathan D, Koepernik K and Pickett W E 2007 *New J. Phys.* **9** 235
[19] Kuneš J, Lukoyanov A V, Anisimov V I, Scalettar R T and Pickett W E 2008 *Nat. Mater.* **7** 198
[20] Wu Z and Cohen R E 2005 *Phys. Rev. Lett.* **95** 037601
[21] Ahart M, Somayazulu M, Cohen R E, Ganesh P, Dera P, Mao H-K, Hemley R J, Ren Y, Liermann P and Wu Z 2008 *Nature* **451** 545
[22] Frantti J, Fujioka Y and Nieminen R M 2008 *J. Phys.: Condens. Matter* **20** 472203
[23] Ganesh P and Cohen R E 2009 *J. Phys.: Condens. Matter* **21** 064225
[24] Kornev I A, Bellaiche L, Bouvier P, Janolin P-E, Dkhil B and Kreisel J 2005 *Phys. Rev. Lett.* **95** 196804
[25] Bousquet E and Ghosez P 2006 *Phys. Rev.* B **74** 180101(R)
[26] González-Vázquez O E and Íñiguez J 2009 *Phys. Rev.* B **79** 064102
[27] Segall M D, Lindan P J D, Probert M J, Pickard C J, Hasnip P J, Clark S J and Payne M C 2002 *J. Phys.: Condens. Matter* **14** 2717
[28] Perdew J P, Burke K and Ernzerhof M 1996 *Phys. Rev. Lett.* **77** 3865
[29] Vanderbilt D 1990 *Phys. Rev.* B **41** R7892
[30] Pfrommer B G, Cote M, Louie S G and Cohen M L 1997 *J. Comput. Phys.* **131** 133
[31] Sani A, Hanfland M and Levy D 2002 *J. Solid State Chem.* **167** 446
[32] Pruzan Ph, Gourdain D, Chervin J C, Canny B, Couzinet B and Hanfland M 2002 *Solid State Commun.* **123** 21
[33] Maignan A, Caignaert V, Raveau B, Khomskii D and Sawatzky G 2004 *Phys. Rev. Lett.* **93** 026401
[34] Hu Z, Wu H, Haverkort M W, Hsieh H H, Lin H J, Lorenz T, Baier J, Reichl A, Bonn I, Felser C, Tanaka A, Chen C T and Tjeng L H 2004 *Phys. Rev. Lett.* **92** 207402
[35] Radaelli P G and Cheong S-W 2002 *Phys. Rev.* B **66** 094408
[36] Gavriliuk A G, Struzhkin V V, Lyubutin I S, Ovchinnikov S G, Hu M Y and Chow P 2008 *Phys. Rev.* B **77** 155112
[37] Imada M, Fujimori A and Tokura Y 1998 *Rev. Mod. Phys.* **70** 1039
[38] Craco L, Laad M S, Leoni S and Rosner H 2008 *Phys. Rev.* B **77** 075108
[39] Kuneš J, Korotin Dm M, Korotin M A, Anisimov V I and Werner P 2009 *Phys. Rev. Lett.* **102** 146402
[40] Lyubutin I S, Ovchinnikov S G, Gavriliuk A G and Struzhkin V V 2009 *Phys. Rev.* B **79** 085125